Available online at www.sciencedirect.com
ScienceDirect
Journal of Photochemistry and Photobiology A: Chemistry 197 (2008) 295–305
Journal of Photochemistry and Photobiology A:Chemistry
www.elsevier.com/locate/jphotochem

A combined experimental and theoretical study on photoinduced intramolecular charge transfer in *trans*-ethyl *p*-(dimethylamino)cinamate

T. Sanjoy Singh [a], S. Mitra [a,*], A.K. Chandra [a], N. Tamai [b], S. Kar [c]

[a] *Department of Chemistry, North-Eastern Hill University, Shillong 793022, India*
[b] *Department of Chemistry, School of Science & Technology, Kwansei Gakuin University, Sanda 669 1337, Japan*
[c] *ChemGen Pharma International, Dr. Siemens Street, Sector V, Salt Lake City, Kolkata 700091, India*

Received 23 November 2007; received in revised form 7 January 2008; accepted 15 January 2008
Available online 20 January 2008

Abstract

Intramolecular charge transfer (ICT) behavior of *trans*-ethyl *p*-(dimethylamino)cinamate (EDAC) in various solvents has been studied by steady-state absorption and emission, picosecond time-resolved fluorescence spectroscopy and femtosecond transient absorption experiments as well as time-dependent density functional theory (TDDFT). Large fluorescence spectral shift in more polar solvents indicates an efficient charge transfer from the donor site to the acceptor moiety in the excited state compared to the ground state. The energy for 0,0 transition ($\nu_{0,0}$) for EDAC shows very good linear correlation with static solvent dielectric property. The relaxation dynamics of EDAC in the excited state can be effectively described by a "three state" model where, the locally excited (LE) state converts into the ICT state within 350 ± 100 fs. A combination of solvent reorganization and intramolecular vibrational relaxation within 0.5–6 ps populates the relaxed ICT state which undergoes fluorescence decay within few tens to hundreds of picoseconds.

Keywords: Charge transfer; Time resolved fluorescence; Femtosecond transient absorption; TDDFT calculation; Vibrational relaxation; Solvent reorganization

1. Introduction

Photoinduced intramolecular charge transfer (ICT) is the most widely studied phenomena in the photophysics of donor (D)–acceptor (A) conjugated systems [1–7]. Molecules of the type D–π–A, where the donor and acceptor groups are connected by single bonds in the opposite sides (*para* position) of a π-conjugated system, often exhibit a large change in dipole moment ($\Delta\mu$) on excitation due to ICT. Since the first observation of ICT phenomenon in 4-(*N*,*N*-dimethylamino)benzonitrile (DMABN) by Lippert et al. [8], many ICT-based aryl amines have been investigated as fluorescence probes [9,10], nonlinear optical materials [11,12], chemical sensors [13,14], two photon absorbing chromophores [15] and electro-optical switches [16]. However, the nature and geometry of the ICT state, even for a simple molecule like DMABN and its derivatives, is still controversial and a subject of great interest [17–20]. Several distinct models have been proposed for the ICT state, including a twisting of the dimethylamino (NMe_2)–benzonitrile (ϕ–CN) single bond that results in a nearly perpendicular D–A geometry (twisted intramolecular charge transfer, TICT) [21–23], an in plane bending of the cyano group (rehybridization by intramolecular charge transfer, RICT) [24], and a pyramidalization (wagged intramolecular charge transfer, WICT) [25] or a planarization (planar intramolecular charge transfer, PICT) of the amino group [26]. Out of all these models, the TICT mechanism is the most widely accepted since it can explain the spectroscopic properties of most of the ICT based arylamines [27,28].

It is also well demonstrated that, in polar protic solvents, specific hydrogen bonding between solvent and electron donor or acceptor groups of the ICT probe often play an important role in the excited state relaxation process [29–32]. Pesquer and co-workers [29] suggested that hydrogen bonding of *para*-substituted *N*,*N*-dialkylanilines with water in the ground state maintains a large twist angle between the donor and acceptor groups, thereby facilitating the ICT process. For another ICT probe, *p*-(*N*,*N*-diethylamino)benzoic acid (DEABA), Kim

* Corresponding author. Tel.: +91 364 272 2634; fax: +91 364 255 0486.
E-mail addresses: smitra@nehu.ac.in, sivaprasadm@yahoo.com (S. Mitra).

1010-6030/$ – see front matter © 2008 Elsevier B.V. All rights reserved.
doi:10.1016/j.jphotochem.2008.01.007

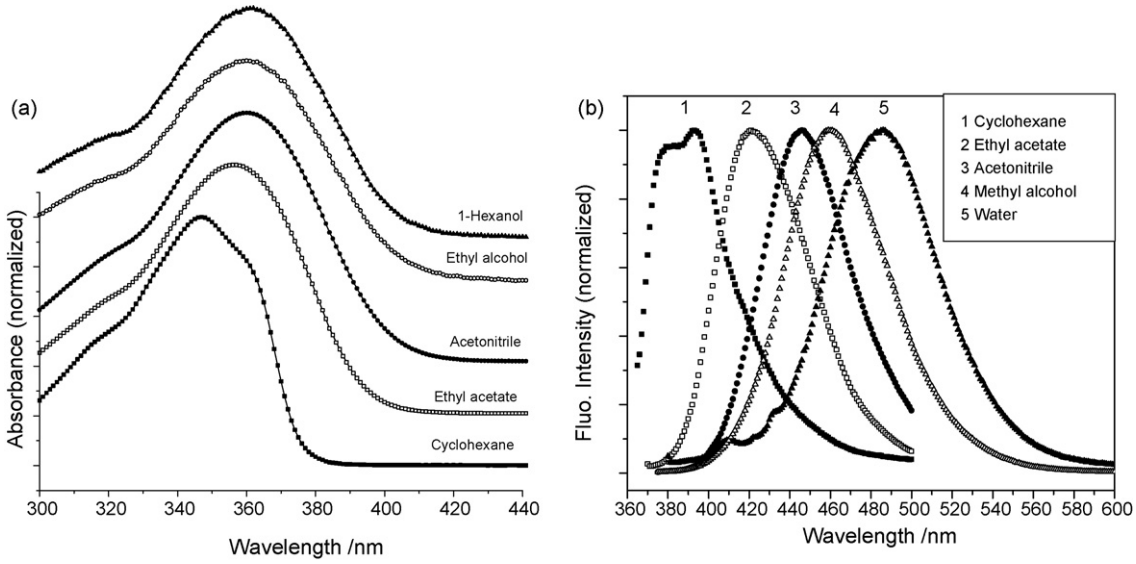

Fig. 1. Electronic absorption (a) and fluorescence emission (b) spectra of EDAC in various solvents.

et al. [30] have shown that specific hydrogen bonding between electron acceptor group and the solvent increases the fluorescence intensity of the ICT state. On the other hand, significant quenching of the charge separated state of *N*,*N*-dimethylaminophenyl(phenyl)acetylene is observed in protic solvents [33]. In a classic paper, Chou et al. [34] have shown that double proton transfer (DPT) as well as charge transfer (CT) behavior in 4-(*N*-substituted amino)-1H-pyrolo[2,3-*b*]pyridines can be modulated by solvent dielectric and hydrogen bonding perturbation.

Recently, photoinduced intramolecular charge transfer reaction of *p*-(dimethylamino)cinnamaldehyde and its derivatives have been reported by steady-state absorption, fluorescence spectroscopy and quantum chemical calculations [35–37]. When compared with DMABN, the possible participation of double bond torsion (*cis–trans* isomerization) in the excited state manifold often complicates the photochemistry of these D–A systems. On the basis of theoretical predictions and steady-state experiments, an emissive TICT state resulting from the twisting of dimethyl amino-phenyl (N–C) single bond has been proposed. The low energy, unstructured, solvent dependent charge transfer emission of *p*-(dimethylamino)cinnamate (EDAC, Scheme 1) was used as an efficient reporter to study protein–surfactant interaction in bovine serum albumin–sodium dodecyl sulfate (BSA–SDS) system as well as micellization behavior of surfactants [38–40]. However, no time-resolved data and corresponding rate parameter was available to address the formation and relaxation of the charge transferred state in varying solvent medium. In the present investigation, we report on TICT phenomenon of EDAC in a variety of pure and mixed solvent systems studied by steady-state absorption and fluorescence measurements, picosecond time resolved fluorescence and femtosecond transient absorption spectroscopic techniques. Theoretical calculations based on time-dependent density functional theory (TDDFT) have also been carried out to support the experimental findings as well as to gain further insight into the potential energy surface of the ground and excited states.

2. Experimental

(*trans*)-Ethyl *p*-(dimethylamino)cinnamate (EDAC) was synthesized using standard procedure based on Reformatsky reaction [41]. The organic solvents used were of spectroscopic grade (>99.5%) as received from Alfa Aesar and, in some cases, from Aldrich Chemical Company. Dielectric constants (ε) and refractive indices (n) of pure solvents were taken from literature [42] and those of the mixed solvents (ε_{MS} and n_{MS}, respectively) were calculated from the volume fractions ($f_i = v_i / \sum v_i$) of the

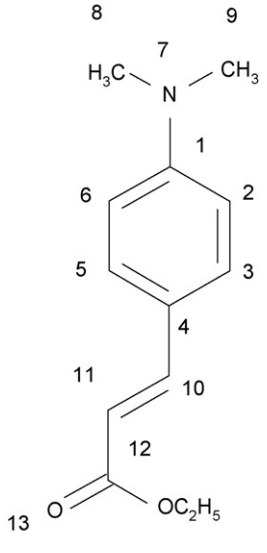

EDAC

Scheme 1. Structure of *trans*-ethyl *p*-(dimethylamino)cinamate. Atom numbering scheme used for the quantum chemical calculations are also shown.

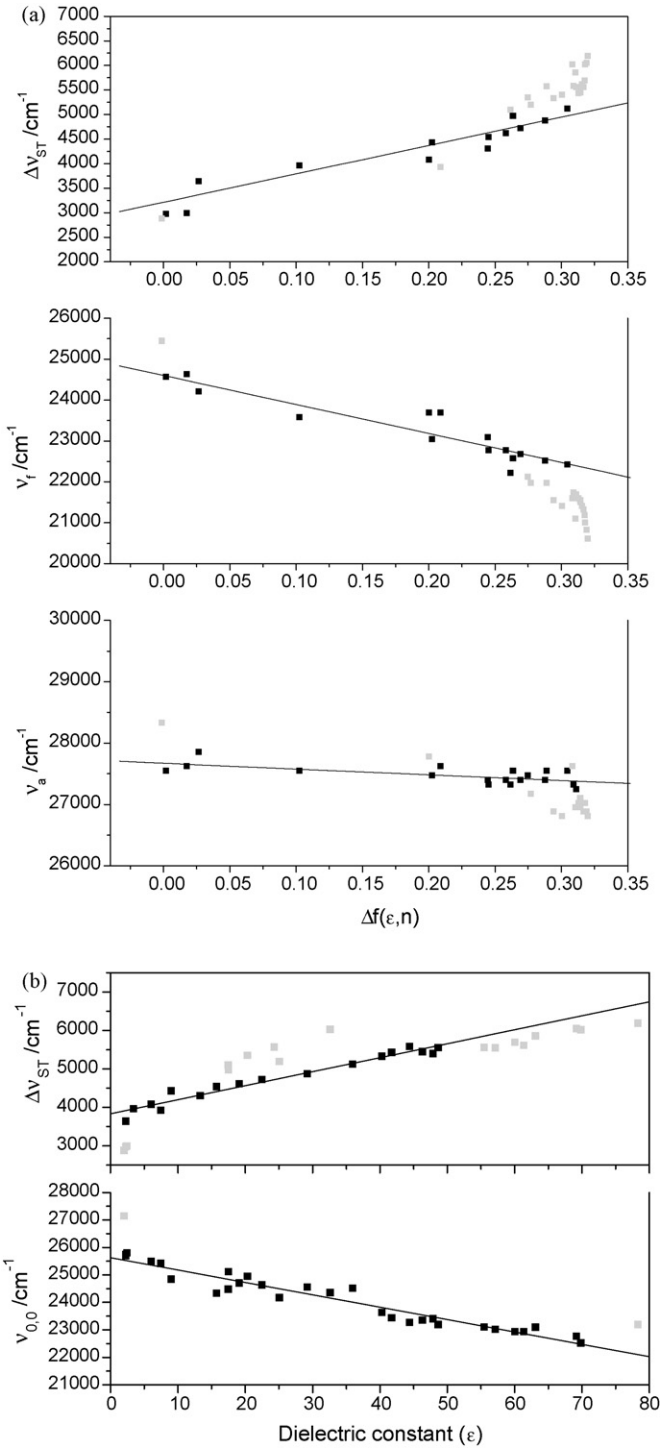

Fig. 2. (a) Plot of absorption energy (ν_a), fluorescence energy (ν_f) and Stokes' shift ($\Delta\nu_{ST}$) against the solvent polarity function $\Delta f(\varepsilon,n)$ for EDAC. (b) Variation of 0,0 transition energy ($\nu_{0,0}$) and Stokes' shift ($\Delta\nu_{ST}$) with solvent static dielectric constants (ε). The light shaded points for protic solvents are excluded from linear regression.

cosolvents (A and B) using following relations [43]

$$\varepsilon_{MS} = f_A\varepsilon_A + f_B\varepsilon_B \quad (1)$$

$$n^2_{MS} = f_A n^2_A + f_B n^2_B \quad (2)$$

Steady-state absorption spectra were recorded on a PerkinElmer model Lambda25 absorption spectrophotometer. Fluorescence spectra were taken in a Hitachi model FL4500 spectrofluorimeter and all the spectra were corrected by measuring the instrument response function both in the excitation and emission side using Rhodamine B and a diffuser (Hitachi part number 650-1576) as the respective standard. Fluorescence quantum yields (ϕ_f) in pure solvents were calculated by comparing the total fluorescence intensity (F) under the whole fluorescence spectral range with that of a standard (quinine sulphate in 1 M sulphuric acid, $\phi_f^s = 0.546$ [44]) using the following equation

$$\phi_f^i = \phi_f^s \frac{F^i}{F^s} \frac{1-10^{-A^s}}{1-10^{-A^i}} \left(\frac{n^i}{n^s}\right)^2 \quad (3)$$

where A^i and A^s are the optical density of the sample and standard, respectively, and n^i is the refractive index of solvent at 293 K. The corresponding value of 1 M sulphuric acid (n^s) is 1.338. For the mixed solvent systems, ϕ_f was calculated using the refractive index calculated by using Eq. (2).

The fluorescence decay curves in different solvents were obtained using time correlated single photon counting (TCSPC) technique. The concentration of the sample was maintained to keep the optical density around 0.1 at the excitation wavelength. The excitation was done at 400 nm obtained by focusing the output (800 nm, 2 MHz repetition rate) of a cavity dumped Ti:Sa laser (Cascade, KMLabs Inc., USA) on 1 mm BBO crystal. The detection system for TCSPC measurements was composed of a monochromator (Japan Spectroscopic, CT-10), a microchannel–plate photomultiplier (Hamamatsu, MCP 2809U), a constant fraction discriminator (Tennelec TC454) and time-to-amplitude converter (Tennelec TC864). The instrument response function for the fluorescence decay measurement was about 30 ps FWHM.

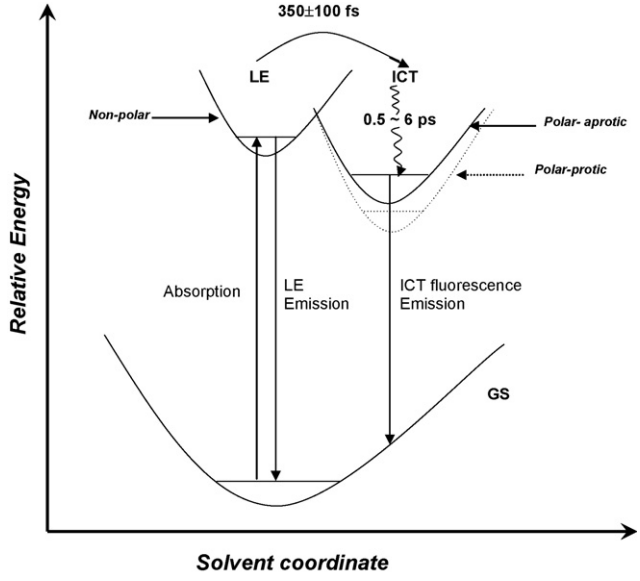

Scheme 2. Schematic energy diagram of solvent dependent excited state photophysics and intramolecular charge transfer phenomena in EDAC along with the corresponding time parameters measured from transient absorption experiments.

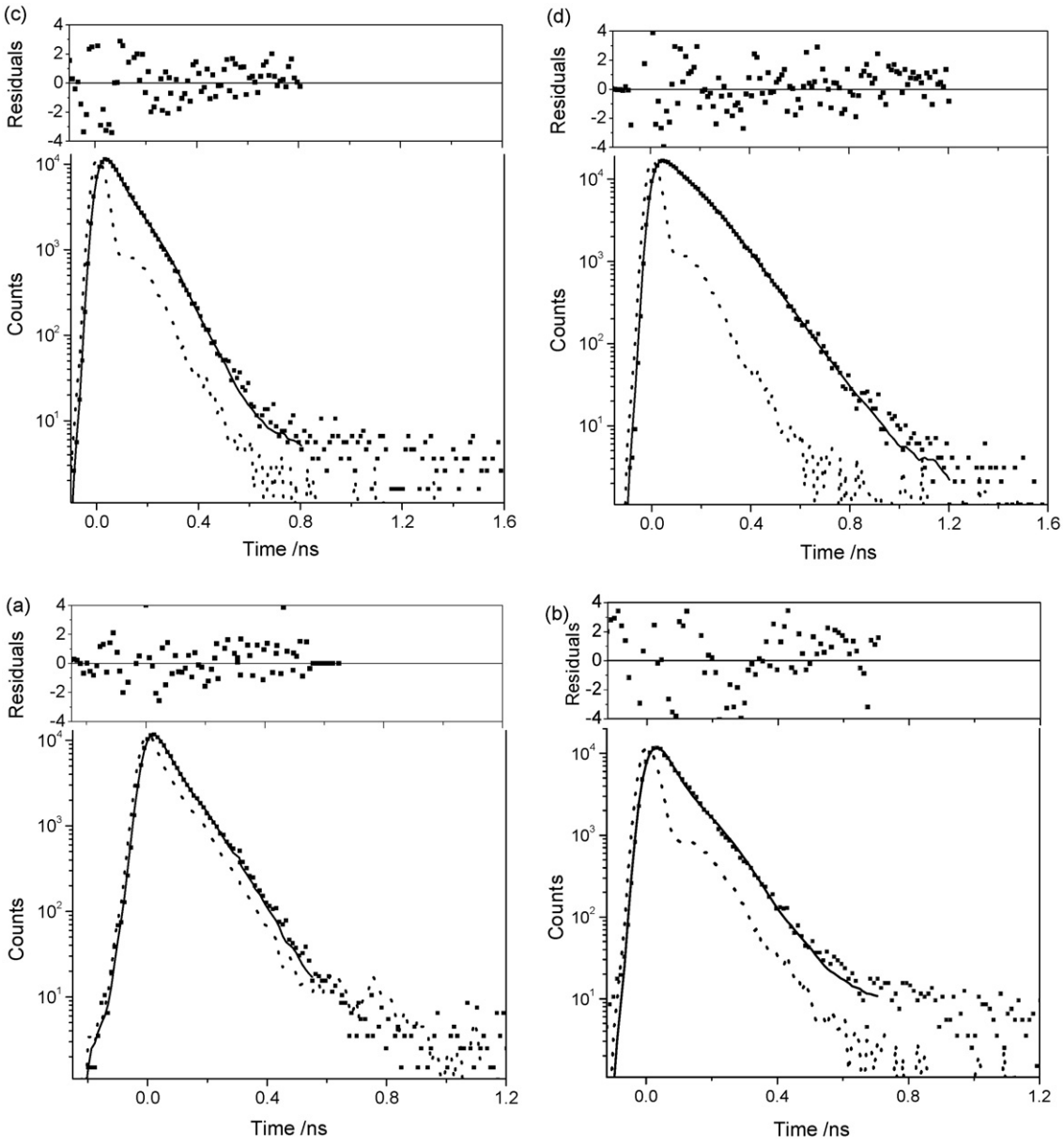

Fig. 3. Typical fluorescence decay profile (scattered points) of EDAC in ethyl acetate (a), toluene (b), tetrahydrofuran (c) and acetonitrile (d) fitted with a single exponential decay function (solid line). The instrument response function (IRF) is also shown by dotted line. The distribution of weighted residual in each case is given in the upper panel.

The laser system for the femtosecond pump–probe experiments was consisted of a Ti:sapphire laser (60 fs, Tsunami, Spectra-Physics) and its amplifier ((Spitfire, Spectra-Physics) that was pumped by a Nd:YLF laser (Merlin, Spectra-Physics). The output of the laser was ~600 mJ at a center wavelength of 780 nm and 1 kHz repetition rate. Eighty percent of a fundamental was used to generate the second harmonic (~390 nm) with a 0.1 mm BBO crystal as an excitation pulse. The remaining 20% of the fundamental was focused into a 1-cm D_2O cell to generate supercontinuum as a probe pulse. The spectrum response function of pump–probe method was estimated to be 200 fs FWHM. The signal was analyzed by a computer-controlled CCD detector (Roper Scientific, SPEC10-100LN and ST-133S controller) at each optical delay using a translation stage (Sigma Koki, SGSP33-200 and Mark 204). The temporal dispersion of supercontinuum was corrected for transient absorption spectra with the same method described elsewhere [45].

The fluorescence decay and one-wavelength transient rise and decay curves were analyzed by nonlinear least-square iterative convolution method based on Lavenberg–Marquardt algorithm.

3. Results and discussion

3.1. Steady-state absorption and emission spectra

The electronic spectra of EDAC display an intense absorption band at around ~360 nm with a shoulder at 320 nm. Fig. 1a shows some of the representative spectra of dilute solutions of this compound and Table 1 contains the corresponding absorption maxima (λ_{abs}) in several solvent systems with varying

Table 1
Steady-state spectral properties of EDAC in various pure and mixed solvent systems

Solvent[a]	$\Delta f(\varepsilon,n)$[b]	λ_{abs} (nm)	λ_{fl} (nm)	$\Delta\nu_{ST}$ (cm^{-1})
Cyclohexane	0.0	353	393	2883
Benzene	0.0	363	407	2978
Toluene	0.02	362	406	2994
1,4-Dioxane	0.03	359	413	3642
1-Octanol	0.10	363	424	3963
Ethylacetate	0.19	360	422	4081
$Ben_{80}Acn_{20}$	0.20	364	434	4431
Tetrahydrofuran	0.21	362	422	3928
1-Hexanol	0.24	365	433	4303
$Ben_{60}Acn_{40}$	0.25	366	439	4543
$Ben_{50}Acn_{50}$	0.26	365	439	4618
$Dio_{80}Wat_{20}$	0.26	366	450	5100
1-Butanol	0.26	363	443	4975
$Ben_{40}Acn_{60}$	0.27	365	441	4722
1-Propanol	0.27	364	452	5349
$Dio_{70}Wat_{30}$	0.28	368	455	5196
$Ben_{20}Acn_{80}$	0.29	365	444	4875
Ethanol	0.29	363	455	5570
$Dio_{50}Wat_{50}$	0.29	372	464	5330
$Dio_{40}Wat_{60}$	0.30	373	467	5396
Acetonitrile	0.30	363	446	5127
Methanol	0.308	362	463	6026
$Acn_{80}Wat_{20}$	0.309	366	460	5583
$Dio_{20}Wat_{80}$	0.310	371	474	5857
$Acn_{70}Wat_{30}$	0.311	367	461	5556
$Met_{80}Wat_{20}$	0.313	370	463	5429
$Acn_{50}Wat_{50}$	0.314	369	464	5549
$Met_{70}Wat_{30}$	0.314	371	465	5449
$Acn_{40}Wat_{60}$	0.315	370	467	5614
$Met_{50}Wat_{50}$	0.317	372	469	5560
$Met_{40}Wat_{60}$	0.317	372	472	5695
$Acn_{20}Wat_{80}$	0.318	370	476	6019
$Met_{20}Wat_{80}$	0.319	372	480	6048
water	0.32	373	485	6191

[a] Abbreviations for the mixed solvent system are Ben (benzene), Acn (acetonitrile), Dio (1,4-dioxane), Wat (water) and Met (methanol). The corresponding volume percentage is mentioned at the suffix.
[b] Calculated using Eq. (6).

polarity. In accordance with the previous reports [38,39], these two bands are assigned to the transition from ground state to the L_a (S_1) and L_b (S_2) state, respectively. The vibrational structure observed for the long wavelength absorption band in cyclohexane is lost in more polar solvents and spectral maxima shifts to red with solvent polarity. However, the solvatochromic shift is rather small (~780 cm^{-1} in acetonitrile relative to cyclohexane) which indicates a small difference between the dipole moments of the Franck-Condon (FC) excited state and the ground state.

The fluorescence emission spectrum is structured in cyclohexane with a maximum at ~390 nm which can be assumed to be originated from the locally excited (LE) state as reported earlier [38]. However, with increasing solvent polarity, the emission becomes structureless and the peak position shows significant red shift (Fig. 1b and Table 1). The large solvatochromic shift of fluorescence emission (~3000 cm^{-1} in acetonitrile relative to cyclohexane) indicates the strong charge transfer character of the fluorescent state in polar solvents. The origin of large solvatochromic fluorescence shift in EDAC can further be substantiated by comparing the solvent dependent fluorescence shift in ethyl 4-nitro-cinnamate (ENC). Due to presence of electron withdrawing nitro group in conjugation with the cinnamate moiety, it is not possible for ENC to show charge transfer emission. It is observed that ENC indeed does not show any notable solvent polarity dependent emission spectra (λ_{em} = 340 and 350 nm in cyclohexane and acetonitrile, respectively).

The excited state dipole moment of LE (μ_{LE}) and CT (μ_{CT}) states can be estimated from the slope of the plots of absorption (ν_a) and fluorescence (ν_f) energies against the solvent polarity parameter, $\Delta f(\varepsilon,n)$, respectively using the following equations [46]

$$\nu_a = \nu_a^0 - \left[\frac{2}{(4\pi\varepsilon_0)(hca^3)}\right] \times [\mu_{LE}(\mu_{LE} - \mu_g)] \times \Delta f(\varepsilon, n) \quad (4)$$

$$\nu_f = \nu_f^0 - \left[\frac{2}{(4\pi\varepsilon_0)(hca^3)}\right] \times [\mu_{CT}(\mu_{CT} - \mu_g)] \times \Delta f(\varepsilon, n) \quad (5)$$

where $\Delta f(\varepsilon,n)$ can be defined as

$$\Delta f(\varepsilon, n) = \frac{\varepsilon - 1}{2\varepsilon + 1} - \frac{n^2 - 1}{2n^2 + 1} \quad (6)$$

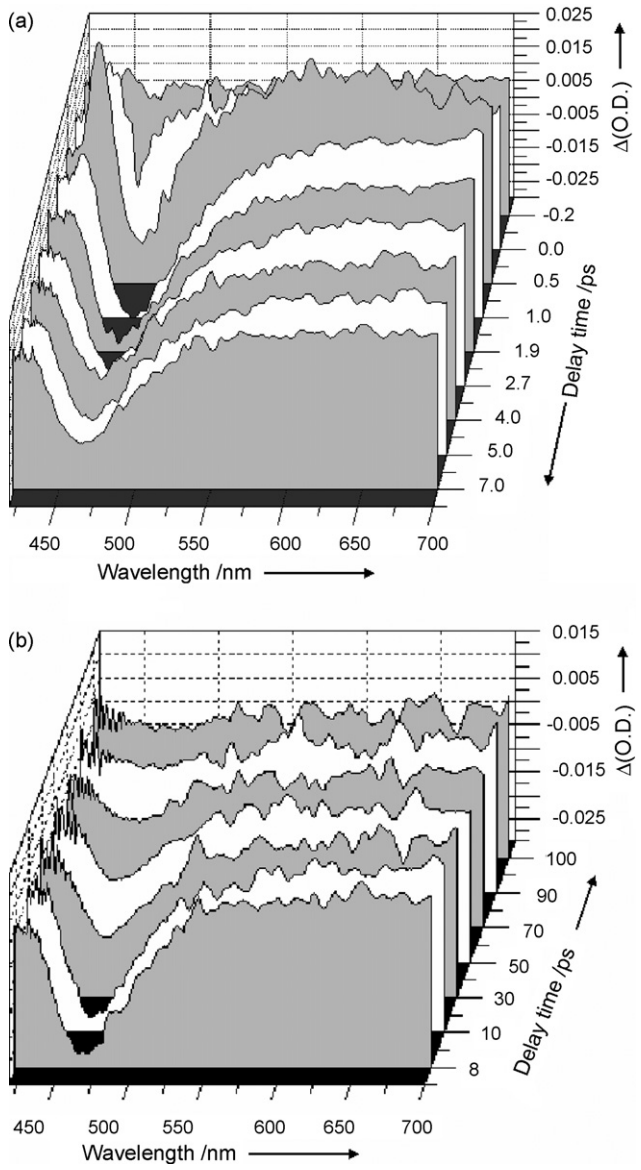

Fig. 4. Variation of transient absorption spectra of EDAC in tetrahydrofuran at very short (a) and long (b) time delay of 400 nm pump and supercontinuum probe pulse.

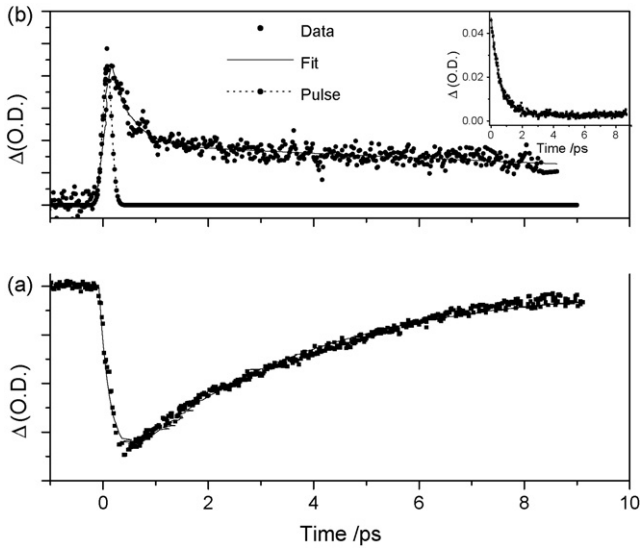

Fig. 5. Simulation of transient absorption intensity of EDAC in acetonitrile at 465 nm (a) and 670 nm (b). Inset shows the fitting of 440 nm transient absorption change with two-exponential decay function.

The value of Onsagar cavity radius "a" (4.9 Å) and the ground state dipole moment (5.1 D) was obtained from the *ab initio* calculations at the HF/6-311++G** level after fully optimizing the geometry at the same level by using Gaussian03 program [47]. Usually, the value of "a" is 0.5 Å larger than the radius corresponding to the molecular volume computed using "Density" keyword in Gaussian03 to account for the van der Waals radii of the surrounding solvent molecules [48].

The magnitude of μ_{LE} and μ_{CT} for EDAC calculated from the slope of the straight lines (Fig. 2a) are 6.7 and 12.0 D, respectively. It is to be mentioned here that during linear fitting, the data related to solvents with appreciable hydrogen bonding ability do not correlate well and consequently, these points were excluded from linear regression (Fig. 2a). So, it is believed that the excited state photophysics of EDAC is strongly perturbed by specific solute–solvent interaction like hydrogen bonding (see below for further discussion) and the behavior of the ICT state in these solvents should be treated separately.

The dipole moment for the charge transfer state (μ_{CT}) can also be calculated from Lippert–Mataga equation (Eq. (7)) [49,50], i.e., from linear variation of Stokes shift ($\Delta\nu_{ST}$) against the solvent parameter, $\Delta f(\varepsilon,n)$ (Fig. 2a)

$$\Delta\nu_{ST} = \Delta\nu_{ST}^{0} + \left[\frac{2}{(4\pi\varepsilon_0)(hca^3)}\right] \times (\mu_{CT} - \mu_g)^2 \times \Delta f(\varepsilon, n) \quad (7)$$

We obtain the value of 13.3 D for EDAC, which is very close to the value (12.0 D) calculated from the solvent polarity effect on fluorescence energy.

It is worth to look for certain spectroscopic quantity that can directly report static dielectric constant (ε) of the medium. In this quest, we checked the variation of Stokes shift ($\Delta\nu_{ST}$) with static dielectric constant (ε) for EDAC in variety of pure solvent and solvent mixtures (details of the solvent system are given in Table 1) with wide range of ε values. It is interesting to note that $\Delta\nu_{ST}$ shows very good linear correlation with ε only when the solvents with appreciable hydrogen bonding ability (like water, methyl alcohol, ethyl alcohol and 1-propanol) or the solvent mixtures containing water as a cosolvent are excluded from the linear regression (Fig. 2b). The higher alcohols are known to have less pronounced hydrogen bonding ability [51] and the Stokes shift in these solvents can be considered to originate only from the polarity effect. This may be a possible explanation for linear variation of $\Delta\nu_{ST}$ with ε even in polar protic solvents like 1-butanol, 1-hexanol or 1-octanol.

However, the energy of the 0,0 transition ($\nu_{0,0}$, the intersection of normalized absorption and emission spectra) shows very good correlation (Eq. (8)) with ε in almost all solvents (Fig. 2b,

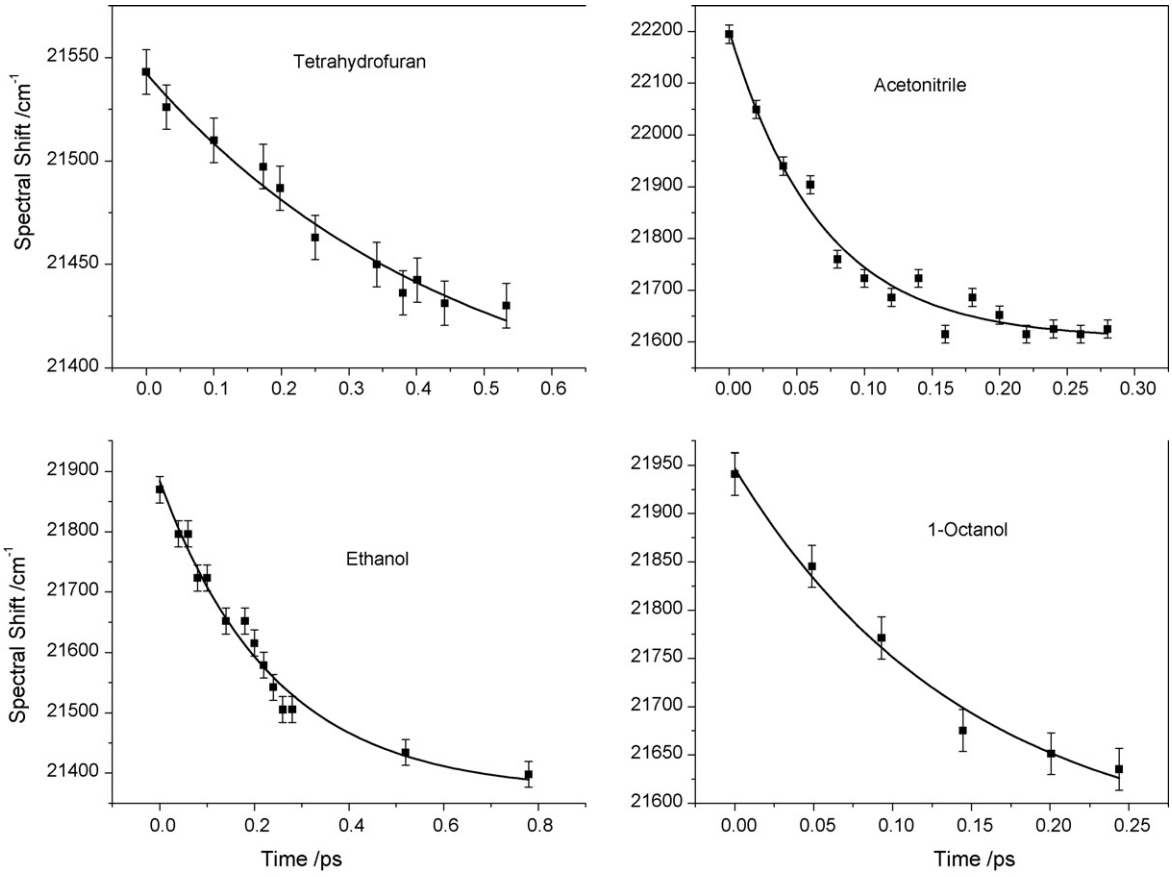

Fig. 6. Time-dependent spectral shift of EDAC stimulated emission in different solvents.

lower panel)

$$\nu_{0,0}\,(\mathrm{cm}^{-1}) = (25628.24 \pm 92.4) + (-45.1 \pm 2.3) \times \varepsilon; \quad R = 0.99 \tag{8}$$

The deviation in cyclohexane is due to the different nature of emission (LE type) when compared with other solvent systems (ICT type). However, the reason for the large deviation in water is not very clear at this point. A possible explanation may be due to extra stabilization of the highly polar ICT state in extensive hydrogen bonded network of water cluster.

3.2. Fluorescence quantum yields and decay times

The fluorescence quantum yields (ϕ_f) of EDAC have been determined in a variety of solvents and the relevant data are reported in Table 2. It is seen that quantum yield for the ICT state increases with solvent polarity upto acetonitrile, however, in presence of hydrogen bonding solvents like water, it decreases substantially. The increase in emission yield is due to the stabilization of the charge transfer state in more polar solvents. However, the decrease of ϕ_f in hydrogen bonding solvents indicates the formation of a new nonradiative decay channel which may be originated due to specific solute solvent interaction. Furthermore, in highly polar solvent, such as water, the formation of the ICT state is favored and stabilized to a great extent because of the very high dipole moment of this state. However, owing to the proximity of the stabilized ICT state and low-lying triplet/ground states, the nonradiative decay is facilitated very much, resulting in appreciable decrease in net ϕ_f.

The fluorescence decay times (τ_f) of EDAC are measured in different solvents at room temperature using time-correlated single photon counting method and the results are also provided in Table 2. All decays could be reproduced with single exponential decay function. Fig. 3 shows some representative fluorescence decays in different solvents. In general, the fluorescence decay time increases with increase in solvent dielectric constant (20 ps in cyclohexane and 101 ps in acetonitrile) in aprotic solvents. A possible explanation for the increase in τ_f may be the rearrangement of electronic excited states with increasing solvent polarity. Radiative (κ_f^r) and nonradiative (κ_f^{nr}) decay rate constants were calculated from the known value of fluorescence quantum yield (ϕ_f) and decay time (τ_f) using the following relation (Eq. (9)) and also given in Table 2

$$\kappa_f^r = \phi_f/\tau_f; \qquad \kappa_f^{nr} = (1-\phi_f)/\tau_f \tag{9}$$

According to Einstein treatment for electronic transition [52,53], the radiative rate constant for spontaneous fluorescence (κ_f^r) is directly proportional to the cube of fluorescence energy (ν_f). Since ν_f shifts to lower energies with increasing solvent polarity, it is expected that the magnitude of τ_f will increase with ε_r. Furthermore, it is seen from Table 2 that the magnitude of $\kappa_f^{nr}s$ is about two orders higher than κ_f^{nr}. Low fluorescence quantum

Table 2
Fluorescence quantum yield (ϕ_f), decay time (τ_f), radiative (κ_f^r) and nonradiative (κ_f^{nr}) decay rate constants of EDAC in different solvents

Solvent	ϕ_f (10^{-3})	τ_f (ps)	κ_f^r(10^8 s^{-1})	κ_f^{nr}(10^{10} s^{-1})
Cyclohexane	6.0	–	–	–
Benzene	11.3	39	2.9	2.5
Toluene	11.9	58	2.1	1.7
Ethyl acetate	15.1	23	6.6	4.3
1,4-Dioxane	14.0	30	4.7	3.3
Tetrahydrofuran	12.1	69	1.8	1.4
Acetonitrile	22.0	101	2.2	1.0
Water	3.2	90	0.4	1.1
Methanol	6.5	75	0.9	1.3
Ethanol	5.7	82	0.7	1.2
1-Propanol	4.3	89	0.5	1.1
1-Butanol	4.0	110	0.4	0.9
1-Hexanol	3.9	118	0.3	0.8
1-Octanol	3.1	129	0.2	0.7

yields and the short excited state fluorescence decay time of EDAC in solutions are direct indications of the nonradiative processes being dominant in the excited state photophysics.

3.3. Dynamics of ICT: transient absorption measurement

The early time dynamics of photophysical processes of EDAC in some of the solvents were studied using 400 nm laser pulse of 60 fs duration for excitation. Fig. 4 shows the evolution of transient signal of EDAC in tetrahydrofuran at different delay times between the pump and probe pulse. The initial broad band in the whole spectral range may be assigned to be originated from $S_n \leftarrow S_1$ absorption from the LE state. The intensity of this broad band decays extremely rapidly with a simultaneous appearance of a negative absorption at around 460 nm. This spectral position is similar to the fluorescence maxima of the ICT state and the negative absorption around this wavelength region can be assigned as originated from the stimulated emission of the ICT state. The time constant for different photophysical processes after initial excitation to the LE state can be obtained from the decay of the initial broad band or from the rise of the corresponding stimulated emission. The variation of transient intensity at specific wavelengths was simulated with 200 fs Gaussian function to isolate these time constants. Fig. 5 shows the variation of transient absorption intensity of EDAC in acetonitrile at 465 nm and 670 nm. It is to be noted here that due to relatively poor signal to noise ratio, the 440 nm transient signal could not be simulated properly. Therefore, the data was fitted with two-exponential decay function in order to extract the time parameters and shown in the inset of Fig. 5. The time constant for the fast decay at 440 nm (280 fs) and 670 nm (300 fs) correlates well with the growth at 465 nm (250 fs, Table 3). This time constant (τ_1) for the growth of the stimulated emission indicates the formation of the ICT state from the LE state and is given in Table 3 for some representative solvent systems. The formation of the ICT state was found to occur within 350 ± 100 fs for different solvents, whereas, the decay of the simulated emission consists of a solvent dependent fast component of 0.5–6 ps (τ_2) along with the natural fluorescence decay time of the ICT state (τ_3) (Table 3).

The time evolution of transient absorption intensity and the rise/decay behavior at selected wavelengths indicate that the excited state photophysics of EDAC is essentially consisting of a three state model, i.e., the ground state, LE state and ICT state (Scheme 2). The later is produced from the LE state after initial excitation of the ground state conformation. The ICT state is characterized by having very high dipole moment compared to the LE state and consequently, is more favored in highly polar solvents. The extremely short-lived LE state acts as a precursor for the formation of the fluorescing ICT state.

The middle component (τ_2) in stimulated emission may be originated due to the combination of two reasons. First, the solvation of the dipolar ICT state can be assumed to be responsible for the origin of τ_2. In most of the solvents, the solvation dynamics occur on a time scale ranging from few hundreds of femtosecond to few tens of picoseconds [2,6,54,55]. The solvation is expected to play a major role in the decay dynamics of stimulated emission because of the large difference in dipole moment between the ground state and ICT state. The other factor that can also be responsible is vibrational relaxation of the ICT state; as for a big molecule like EDAC, the time constant for vibrational relaxation may be within 1–10 ps [56,57]. The effect of vibrational relaxation is generally manifested in the shift of transient absorption spectral peak. We have monitored the time-dependent spectral shift of the stimulated emission (Fig. 6) and the corresponding time constants (τ_{shift}) are also given in the last column of Table 3. It is observed that the effect of vibrational relaxation is complete within few hundreds of femtoseconds for EDAC in all the solvents and a comparison of τ_{shift} with τ_2 indicates that solvent reorganization contributes as a major component in the relaxation dynamics of ICT state, particularly in alcohols.

3.4. Quantum chemical calculations

3.4.1. Ground state structure of EDAC: planar or pyramidal dimethyl amino group?

It was reported earlier that a minimum of 6-31G* or D95** basis set in either HF or DFT method is necessary to reproduce the experimental geometrical parameters for DMABN and a series of other dimethylamino substituted compounds

Table 3
Rise and decay parameters of the stimulated emission for EDAC in different solvents[a]

Solvent	τ_1 (fs) (α_1)	τ_2 (ps) (α_2)	τ_3[b] (ps) (α_3)	τ_{shift} (fs)
Tetrahydrofuran	480 (−0.85)	0.5 (0.63)	70 (0.37)	450
Acetonitrile	250 (−0.9)	0.6 (0.7)	100 (0.3)	<100
Ethanol	400 (−0.92)	4.8 (0.35)	80 (0.65)	250
1-Octanol	350 (−0.85)	5.7 (0.3)	130 (0.7)	150

[a] Values in the parenthesis are the pre-exponential factors (α) associated with each decay time (τ). The time constant for the shift of stimulated emission peak (τ_{shift}) are given in the last column.
[b] These values are taken from the fluorescence decay time (Table 2) and kept fixed during analysis.

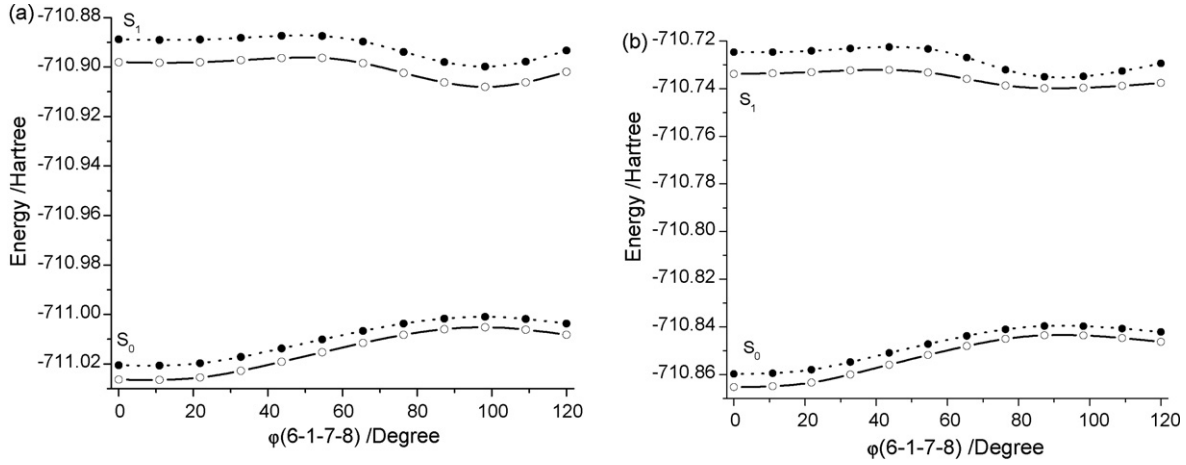

Fig. 7. Potential energy diagram of S_0 and S_1 states of EDAC along the twist coordinate as obtained by TD-B3LYP calculation using 6-311++G** (a) and cc-pVDZ (b) basis sets in cyclohexane (solid circle) and acetonitrile (open circle).

[58]. Furthermore, correct description of the geometry, particularly orientation of the dimethylamino group with rest of the molecule, is important to describe the donor–acceptor properties. Here we have chosen a larger Pople-type 6-311++G** and correlation consistent cc-pVdz basis sets both in Hartree-Fock (HF) and the B3LYP density functional methods. The optimized ground state geometrical parameters of EDAC are reported in Table 4. It is interesting to note that the bond length parameters are remarkably insensitive both towards the method of calculation and nature of the basis set used. However, the notable difference is found in the HF and B3LYP results for the orientation of dimethylamino group with respect to the phenyl ring. The HF method predicts a pyramidal structure with an angle of 12–13° for the torsional angle φ(6-1-7-8), whereas, the B3LYP method produces relatively more planar structure (ca. 6–8°) with both the basis sets. Similar results were reported previously for other dimethylamino group based donor–acceptor systems [37,58] and conclusion was made for a pyramidal structure at the nitrogen center in the ground state. However, careful analysis of our results shows that ground state rotation of C1–N7 bond is essentially free within the range of 0–20° at room temperature. For example, B3LYP/6-311++G** calculation for EDAC

Table 4
Ground state optimized geometric parameters of EDAC in HF and B3LYP method using 6-311++G** and cc-pVDZ basis sets[a]

Parameters[b]	HF		B3LYP	
	6-311++G**	cc-pVDZ	6-311++G**	cc-pVDZ
r(1-7)	1.384	1.383	1.383	1.382
r(4-10)	1.473	1.469	1.458	1.461
r(10-11)	1.336	1.334	1.349	1.352
r(11-12)	1.484	1.483	1.474	1.473
r(12-13)	1.194	1.193	1.217	1.221
θ(8-7-9)	116.5	117.0	118.2	119.0
θ(1-7-9)	118.9	119.1	119.9	120.0
θ(1-7-8)	118.8	118.9	119.8	119.9
φ(6-1-7-8)	13.2	12.3	8.2	5.9
φ(6-1-7-9)	165.8	166.7	171.8	174.1

[a] See Scheme 1, for atom numbering.
[b] Bond lengths (r) in Å, bond angles (θ) and dihedrals (φ) are in degree.

predicts that the ground state structures with fixed φ(6-1-7-8) at 0° and 20° are only about 0.25 and 0.57 kcal mol^{-1} higher in energy than the fully optimized structure. Therefore, it can be assumed that different conformations can exist with varying φ(6-1-7-8) angle within this range (0–20°) in the ground state and pyramidal structure at the nitrogen centre is not an essential criterion for these types of molecules to show ICT behavior.

3.4.2. Characterization of excited state

To characterize the excited state, we have used both the HF-CIS method and TDDFT along with the 6-311++G** and cc-pVDZ basis sets. The SCRF/SCIPCM model as implemented in Gaussian03 is used to include the solvent effect in transition energies [47]. Our calculations in gas phase, as well as in solvent, indicate that the maximum absorption observed at ~360 nm in the experiment corresponds to the $S_1(\pi\pi^*)$ state. The transition energy to this state in cyclohexane is found to be 3.58 eV at TD-B3LYP/6-311++G** level and 3.67 eV at TD-B3LYP/cc-pVDZ level. The analysis of TDDFT wavefunction indicates that the transition to the S_1 state has pure $\pi \rightarrow \pi^*$ (HOMO → LUMO) characteristics with appreciably high oscillator strength ($f > 0.8$). In contrast, the HF-CIS/6-311++G** calculation predicts that the S_1 state has an energy of 4.69 eV relative to the ground state, which is very far from the experimentally obtained value of 353 nm (3.51 eV) as mentioned in Table 1. Consequently, TD-B3LYP method was chosen to construct the potential energy surface for the ICT state as discussed below. Further to verify the applicability of the quantum chemical calculation and assignment of the absorption peaks described before, the oscillator strength was calculated from the integrated absorption intensity using the following relation [59]:

$$f = \frac{(4.39 \times 10^{-9})}{n} \int \varepsilon(\nu)\, \mathrm{d}(\nu) \tag{10}$$

where n is the refractive index of the medium. The experimental value (~0.6) is in very good agreement with the theoretically calculated value (~0.8) for $S_0 \rightarrow S_1$ transition of EDAC obtained by TD-B3LYP/6-311++G** level of calculation.

It is to be noted here that the theoretically calculated value for the S_2 transition energy is 4.23 eV (~295 nm). The agreement with the experimental value (~320 nm) is not as good as observed for the S_1 state. However, this discrepancy is expected due to the fact that it becomes increasingly more difficult to represent the higher excited states with the level of quantum mechanical approximation used in this study.

3.4.3. Potential energy surface for ICT state

The potential energy surface with varying twist angles, φ(6-1-7-8), for both the ground and excited state, as obtained from the TD-B3LYP calculations using both 6-311++G** and cc-pVDZ basis sets in cyclohexane and acetonitrile, are shown in Fig. 7. It is observed that the ground state energy rises to about 12.3 kcal mol^{-1} with increasing the twist angle to 100° relative to the global minimum. Therefore, rotation around C1–N7 bond towards the formation of the ICT structure in the ground state is unlikely. However, in the S_1 state, the PES is found to be rather flat with a shallow minimum at about 100° twist angle. Consequently, the formation of the fluorescing twisted structure becomes energetically viable and spontaneous in the excited state, as observed experimentally. From Fig. 7, it is also seen that the stabilization of the excited state in polar acetonitrile is relatively larger in excited state compared to the ground state. This indicates that the dipole moment in the excited state is higher than the ground state and it further substantiates the experimental results discussed in the previous sections.

4. Conclusion

The excited state photophysics of EDAC has been reported in different pure and mixed solvent systems. Large bathochromic shift in the fluorescence spectra with increasing solvent polarity indicates strong charge transfer nature of the excited state. The dipole moments for the LE and ICT states were calculated from the linear variation of absorption and fluorescence energy with solvent polarity parameter as well as from Lippert–Mataga plot. The energy for (0,0) transition shows very good correlation with static dielectric parameter of the solvent. The life time of the ICT state increases with polarity of the solvents due to the greater stabilization of the charge transferred state. Ultrafast transient absorption measurements reveal that the formation of the ICT state from the LE state occurs within 350 ± 100 fs and solvent reorganization plays a major role in the excited state decay dynamics along with intramolecular vibrational relaxation. Quantum chemical calculations predict a nearly pyramidal ground state geometry of the dimethylamino group to the rest of molecule, although possibility of different orientations within 0–20° could not be ruled out within accessible thermal energy. The potential energy curves constructed from the B3LYP calculations for the ground and excited states along the twist coordinate corroborate the experimental observation that formation of ICT state is only feasible in the excited state, not in the ground state.

Acknowledgments

Financial support from Council of Scientific & Industrial Research (CSIR) and Department of Science & Technology (DST), Government of India is gratefully acknowledged. The authors would like to thank Dr. Wang Li, Department of Chemistry, Kwansei Gakuin University for her help in measuring the femtosecond transient absorption data. S. Mitra thanks Kwansei Gakuin University for partially supporting his travel expenses during summer visit in Japan.

References

[1] J.S. Yang, K.L. Liau, C.M. Wang, C.Y. Hwang, J. Am. Chem. Soc. 126 (2004) 12325.
[2] A.K. Singh, G. Ramakrishna, H.N. Ghosh, D.K. Palit, J. Phys. Chem. A 108 (2004) 2583.
[3] K. Bhattacharyya, M. Chowdhury, Chem. Rev. 93 (1993) 507.
[4] S. Nad, M. Kumbhakar, H. Pal, J. Phys. Chem. A 107 (2003) 4808.
[5] M. Maus, W. Rettig, J. Phys. Chem. A 106 (2002) 2104.

[6] N. Tamai, T. Nomoto, F. Tanaka, Y. Hirata, T. Okada, J. Phys. Chem. A 106 (2002) 2164.
[7] W. Verbouwe, L. Viaene, M. Van der Auweraer, F.C. De Schryver, H. Masuhara, R. Pansu, J. Faure, J. Phys. Chem. A 101 (1997) 8157.
[8] E. Lippert, W. Lüder, H. Boss, in: A. Mangini (Ed.), Advances in Molecular Spectroscopy, Pergamon, Oxford, 1962, p. 443.
[9] P. Das, A. Mallick, A. Chakravarty, B. Halder, N. Chattopadhyay, J. Chem. Phys. 125 (2006) 44516.
[10] K.D. Ashby, K. Das, J.W. Petrich, Anal. Chem. 69 (1997) 1925.
[11] T. Verbiest, D.M. Burland, M.C. Jurich, V.Y. Lee, R.D. Miller, W. Volksen, Science 268 (1995) 1604.
[12] S.R. Marder, J.W. Perry, Science 263 (1994) 1706.
[13] J.S. Yang, Y.D. Lin, Y.H. Lin, F.L. Liao, J. Org. Chem. 69 (2004) 3517.
[14] T. Morozumi, T. Anada, H. Nakamura, J. Phys. Chem. B 105 (2001) 2923.
[15] M. Albota, D. Beljonne, J.L. Brédas, J.E. Ehrlich, J.Y. Fu, A.A. Heikal, S.E. Hess, T. Kogez, M.D. Levin, S.R. Marder, D. McCord-Maughon, W.J. Perry, H. Röckel, M. Rumi, G. Subramaniam, W.W. Web, X.L. Wu, C. Xu, Science 281 (1998) 1653.
[16] J.J. La Clair, Angew. Chem. Int. Ed. 38 (1999) 3045.
[17] S. Cogan, S. Zilberg, Y. Haas, J. Am. Chem. Soc. 128 (2006) 3335.
[18] K. Dahl, R. Biswas, N. Ito, M. Maroncelli, J. Phys. Chem. B 109 (2005) 1563.
[19] V.I. Tomin, A. Krzysztofowicz, J. Photochem. Photobiol. A: Chem. 172 (2005) 1.
[20] K.A. Zachariasse, S.I. Druzhinin, W. Bosch, R. Machinek, J. Am. Chem. Soc. 126 (2004) 1705.
[21] K. Rotkiewicz, K.H. Grellmann, Z.R. Grabowski, Chem. Phys. Lett. 19 (1973) 315.
[22] W. Rettig, B. Bliss, K. Dirnberger, Chem. Phys. Lett. 305 (1999) 8.
[23] Z.R. Grabowski, K. Rotkiewicz, Chem. Rev. 103 (2003) 3899.
[24] A.L. Sobolewski, W. Domcke, Chem. Phys. Lett. 259 (1996) 119.
[25] W. Schuddeboom, S.A. Jonker, J.M. Warman, U. Leinhos, W. Kühnle, K.A. Zachariasse, J. Phys. Chem. 96 (1992) 10809.
[26] A. Demeter, K.A. Zachariasse, Chem. Phys. Lett. 380 (2003) 699.
[27] D. Pines, E. Pines, W. Rettig, J. Phys. Chem. A 107 (2003) 236.
[28] J. Dobkowski, J. Wojcik, W. Kozminski, R. Kols, J. Waluk, J. Michl, J. Am. Chem. Soc. 124 (2002) 2406.
[29] C. Cazeau-Dubruco, S.A. Lyazidi, P. Canbou, A. Peirigua, Ph. Cazeau, M. Pesquer, J. Phys. Chem. 93 (1989) 2347.
[30] Y.H. Kim, H.W. Cho, M. Yoon, N.W. Song, D. Kim, Chem. Phys. Lett. 264 (1997) 673.
[31] L. Biczók, T. Yatsuhashi, T. Bérces, H. Inoue, Phys. Chem. Chem. Phys. 3 (2001) 980.
[32] M. Józefowicz, K.A. Kozyra, H.R. Heldt, J. Heldt, Chem. Phys. 320 (2005) 45.
[33] Y. Hirata, T. Okada, T. Nomoto, J. Phys. Chem. A 102 (1998) 6585.
[34] P.T. Chou, Y.-I. Liu, H.-W. Liu, W.-S. Yu, J. Am. Chem. Soc. 123 (2001) 12119.
[35] S. Panja, P. Chowdhury, S. Chakravorti, Chem. Phys. Lett. 368 (2003) 654.
[36] P.R. Bangal, S. Chakravorti, J. Photochem. Photobiol. A: Chem. 116 (1998) 191.
[37] A. Chakraborty, S. Kar, N. Guchhait, Chem. Phys. 320 (2006) 75.
[38] T.S. Singh, S. Mitra, J. Lumin. 127 (2007) 508.
[39] R. Das, D. Guha, S. Mitra, S. Kar, S. Lahiri, S. Mukherjee, J. Phys. Chem. A 101 (1997) 4042.
[40] T.S. Singh, S. Mitra, J. Colloid Interface Sci. 311 (2007) 128.
[41] A. Vogel, Textbook of Practical Organic Chemistry, 4th ed., ELBS, 1978, p. 535.
[42] J.A. Dean (Ed.), Lange's Handbook of Chemistry, 13th ed., Mcgraw-Hill, New York, 1987.
[43] S. Nad, H. Pal, J. Phys. Chem. A 105 (2001) 1097.
[44] J.N. Demas, G.A. Crosby, J. Phys. Chem. 75 (1971) 991.
[45] N. Tamai, T. Asahi, H. Masuhara, Rev. Sci. Instrum. 64 (1993) 2496.
[46] F.D. Lewis, W. Weigel, J. Phys. Chem. A 104 (2000) 8146.
[47] M.J. Frisch, et al., Gaussian 03, revision D.01, Gaussian, Inc., Wallingford, CT, 2004.
[48] J.B. Foresman, Æ. Frisch, Exploring Chemistry with Electronic Structure Methods, 2nd ed., Gaussian, Inc., Pittsburgh, PA, 1996.
[49] E. Lippert, Z. Elecktrochem. 61 (1957) 962.
[50] N. Mataga, Y. Kaifu, M. Koizumi, Bull. Chem. Soc. Jpn. 29 (1956) 465.
[51] Y. Marcus, Chem. Soc. Rev. 22 (1993) 409.
[52] J.B. Birks, Photophysics of Aromatic Molecules, Wiley-Interscience, New York, 1983.
[53] J.R. Lakowicz, Principles of Fluorescence spectroscopy, Plenum Press, New York, 1983.
[54] L. Reynolds, J.A. Gardecki, S.J.V. Frankland, M.L. Horng, M. Maroncelli, J. Phys. Chem. 100 (1996) 10337.
[55] S.J. Rosenthal, X.L. Xie, M. Du, G.R. Fleming, J. Chem. Phys. 95 (1991) 4715.
[56] Y. Kimura, J.C. Alfano, P.K. Walhout, P.F. Barbara, J. Phys. Chem. 98 (1994) 3450.
[57] G. De Belder, G. Schweitzer, S. Jordens, M. Lor, S. Mitra, J. Hofkens, S. De Feyter, M. Van der Auweraer, A. Herrmann, T. Weil, K. Müllen, F.C. De Schryver, Chem. Phys. Chem. 1 (2001) 49.
[58] R. Schamschule, A. Parusel, G. Köhler, J. Mol. Struc. (Theochem) 419 (1997) 161.
[59] R.J. Silbey, R.A. Alberty, Physical Chemistry, 3rd ed., John Wiley & Sons (Asia) Pte. Ltd., Singapore, 2002, p. 517.